Polymer Therapeutics

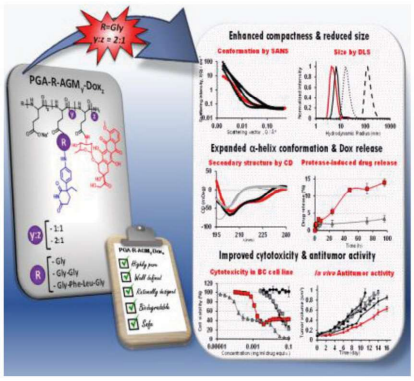

A complex interplay of physical factors drives the interaction between nanomaterials and the biointerface. A panel of physicochemical descriptors has allowed to establish a structure–anticancer activity relationship of a wide family of biodegradable polyglutamate–drug conjugates, bearing synergistic loadings of chemotherapeutic and endocrine agents, highlighting the crucial role of a small glycine drug linker.

ADVANCED FUNCTIONAL MATERIALS
www.afm-journal.de

Anticancer Activity Driven by Drug Linker Modification in a Polyglutamic Acid-Based Combination-Drug Conjugate

Juan J. Arroyo-Crespo, Coralie Deladriere, Vicent J. Nebot, David Charbonnier, Esther Masiá, Alison Paul, Craig James, Ana Armiñán,* and María J. Vicent*

Combination nanotherapies for the treatment of breast cancer permits synergistic drug targeting of multiple pathways. However, poor carrier degradability, poor synergism of the combined drugs, low drug release regulation, and a lack of control on final macromolecule solution conformation (which drives the biological fate) limit the application of this strategy. The present study describes the development of a family of drug delivery systems composed of chemotherapeutic (doxorubicin) and endocrine therapy (aromatase inhibitor aminoglutethimide) agents conjugated to a biodegradable poly-L-glutamic acid backbone via various linking moieties. Data from in vitro cytotoxicity and drug release assessments and animal model validation select a conjugate family member with optimal biological performance. Exhaustive physicochemical characterization in relevant media (including the study of secondary structure, size measurements, and detailed small-angle neutron scattering analysis) correlates biological data with the intrinsic supramolecular characteristics of the conjugate. Overall, this study demonstrates how a small flexible Gly linker can modify the spatial conformation of the entire polymer–drug conjugate, promote the synergistic release of both drugs, and significantly improve biological activity. These findings highlight the need for a deeper understanding of polymer–drug conjugates at supramolecular level to allow the design of more effective polymer–drug conjugates.

1. Introduction

Combination anticancer strategies within nanomedicine may represent an efficient means to treat breast cancer,[1,2] a molecularly complex and heterogeneous disease that often metastasizes and/or becomes drug resistant.[3] There currently exist a wide range of strategies under investigation, including the liposomal entrapment of Cytarabine and Daunorubicin (FDA approved Vyxeos, formerly CPX-351), which has improved all efficacy parameters, including overall survival, in a Phase 3 clinical trial of high-risk acute myeloid leukemia patients.[4]

Polymeric therapeutics (PT) as single agent or as combination therapeutics offer numerous advantages over conventional drugs, including the possibility of an enhanced passive accumulation via the enhanced permeability and retention (EPR) effect on those tumors adequately vascularized,[5] or the ability to cross specific biological barriers.[6] Moreover, drug(s) conjugation to a polymeric carrier benefits from several additional advantages[7,8] as an optimized drug pharmacokinetics, multivalence that allows the conjugation of multiple active/imaging agents and targeting moieties,[2,9] and the ability to target drug activity to tumors via bioresponsive polymer–drug linkers.[10] One issue limiting the widespread use of polymer conjugates is the current lack of understanding of the complex interplay of dynamic physicochemical factors, such as size, shape, surface chemistry, roughness, rigidity, and the influence of linkers and active agents, which characterize the interaction of nanosized PTs with the biological interface.[11]

We developed the first polymer–drug combination conjugate, an *N*-(2-hydroxypropyl) methacrylamide copolymer carrying both aminogluthetimide and doxorubicin (HPMA-AGM-Dox), with the aim of combining an aromatase inhibitor with a chemotherapeutic agent for the treatment of chemotherapy-resistant breast cancer.[12–14] HPMA-AGM-Dox displayed enhanced in vitro breast cancer cell toxicity compared to a combination of the unconjugated drugs or individual polymer–drug conjugates.[12,13] Recently, in vivo proof of concept for antitumor drug synergism with the combination conjugate has been also achieved in an aggressive metastatic 4T1 murine breast cancer model.[14] The mechanism of the enhanced activity appeared primarily due to the kinetics of drug release and the fact that both drugs were made "bioavailable" in the same cell at the same time. Importantly, when protein expression of tumor tissue samples were

J. J. Arroyo-Crespo, Dr. C. Deladriere,[+] Dr. V. J. Nebot, D. Charbonnier, E. Masiá, Dr. A. Armiñán, Dr. M. J. Vicent
Polymer Therapeutics Laboratory
Centro de Investigación Príncipe Felipe
Av. Eduardo Primo Yúfera 3, Valencia 46012, Spain
E-mail: aarminan@cipf.es; mjvicent@cipf.es
D. Charbonnier, E. Masiá, Dr. M. J. Vicent
Screening Platform
Centro de Investigación Príncipe Felipe
Av. Eduardo Primo Yúfera 3, Valencia 46012, Spain
Dr. A. Paul, C. James
School of Chemistry
Cardiff University
Main Building, Park Place, Cardiff CF103AT, UK
The ORCID identification number(s) for the author(s) of this article can be found under https://doi.org/10.1002/adfm.201800931.
[+]Present address: PCAS Canada, 725 Trotter Street, St Jean sur Richelieu, QC J3B 8J8, Canada
DOI: 10.1002/adfm.201800931

analyzed, strong differences were observed in tumor-associated angiogenesis pathways, which could only be explained by the simultaneous estrogen inhibition induced by AGM, only made available at the appropriate cell and time with the combination conjugate. This effect was enhanced by an autophagic cell death mechanism only associated with the combination conjugate.[14] These results demonstrated for the first time that the rational design of a combination PT could significantly enhance drug therapeutic output while also significantly reducing the side effects and tissue damage observed when applying the unconjugated forms of these active agents. This concept has been further explored and reinforced both in vitro and in vivo through studies in our laboratory and other research groups.[2]

However, despite these promising findings, preclinical evidence of detrimental side effects derived from the chronic use of biopersistent polymer carriers (i.e., HPMA or polyethylene glycol, PEG)[15] have led to an exponentially growing research interest on biodegradable polymers, in particular, polypeptides such as poly-L-glutamic acid (PGA)[10,16] as clinical benefits have been achieved with polypeptide based polymeric drugs, such as Copaxone[17] (one of the top ten selling drugs)[8,18] and the lessons learnt with PGA-based anticancer PTs such as Opaxio.[19]

Encouraged by the successful application of PGA to conjugate chemotherapy as single agents[19] and in combination,[20,21] as well as our prior data combining endocrine and chemotherapy,[12–14] we now describe the first PGA-based combination conjugates bearing chemotherapy and estrogen modulator agents for the treatment of breast cancer. Furthermore, we took this opportunity to explore how the incorporation of different polymer–drug linkers influences conjugate characteristics and biological fate. Implementing a rational experimental design, we systematically prescreened a family of single and combination conjugates, provided with different drug loadings and linkers, in vitro in a breast cancer cell line, and then selected successfully screened conjugates for further assessments in an aggressive orthotopic 4T1 breast cancer murine model. We also studied the spatial conformation and physical structure of our conjugate family in biological milieu to predict and better understand intrinsic interactions with the nanobiointerface and therefore, therapeutic effect and mechanisms of action. Parameters assessed included drug release kinetics in the presence of lysosomal enzymes as well as 3D conformation including secondary structure, size, and shape by dynamic light scattering (DLS), small angle neutron scattering (SANS), and circular dichroism (CD). We present the selected PGA-based drug-combination conjugate as an exciting therapeutic candidate, underlining that the choice and/or design of drug–polymer linkers may allow tight spatiotemporal control of drug release and the enhanced personalized treatment of aggressive breast cancer.

2. Results and Discussion

2.1. Synthesis and Characterization of Polymer–Drug Conjugates

We employed optimized and scalable synthetic methodologies to develop a rationally designed family of polymer-based combination anticancer conjugates using *n*-butyl PGA (100 units, $M_w \approx 13$ kDa) as a biodegradable carrier, with the aim of achieving drug synergism. Aromatase inhibitors, such as aminoglutethimide (AGM), induce apoptosis[22] and can act synergistically when combined with chemotherapeutics,[23] as previously shown in our studies with HPMA-based combination conjugates.[12–14] Although HPMA has demonstrated its suitability as carrier for anticancer treatments, we expected that replacing HPMA with PGA would improve safety issues specially in chronic administrations given its enhanced biodegradability. This improved characteristic would reduce unwanted side effects related to polymer accumulation as seen with other nonbiodegradable carrier such as PEG.[15,24]

Therefore, we developed a library of well-defined PGA-conjugates via carbodiimide coupling (**Figure 1**).[12,25] We also synthesized and fully characterized single-agent PGA conjugates bearing Dox or AGM for comparative purposes (**Table 1** summarizes data on all conjugates assessed). We introduced Dox directly and AGM via direct amide conjugation, a Gly linker (G),[26] a Gly–Gly linker (GG),[27] or the well-known tetrapeptidic Gly-Phe-Leu-Gly linker (GFLG), which is cleaved by the lysosomal thiol-dependent protease Cathepsin B.[28] To explore the effect of two different therapeutic scenarios, we fixed Dox content within the polymer conjugate at 5% mol, but varied AGM from 5% mol (low loading [$_{LL}$]) to 10% mol (high loading [$_{HL}$]) (Figure 1A). Additionally, we also incorporated both drugs within the same PGA chain to create a family of combination conjugates. Importantly, the robust methodology employed and tight controls on drug loading permitted the scale-up of this process to gram-scale batches without losses in either conjugation efficiency or yield. Prior to characterization, we isolated and purified all conjugates by size exclusion chromatography (SEC) to remove any excess of salts, activating agents or traces of unreacted drugs (see 1C, Supporting Information, for a detailed synthetic methodology).

^{1}H NMR characterization of the synthesized products was used to determine their identity and purity. As demonstrated in Figure 1B, which displays spectra of representative conjugates, the covalent incorporation of a single drug (PGA-(G-AGM)$_{LL}$, PGA-Dox), or the drug combination (PGA-(G-AGM)$_{LL}$-Dox) into the polymer backbone resulted in the expected widening of characteristic drug signals (see Figures S11 and S12, Supporting Information, for details on family characterization). The signal of the Dox methylene group at 1.2 ppm and the signals corresponding to the aromatic ring (0.75 ppm) and ethylene group (7.4 ppm) of AGM permitted identity verification for both the single and combination nanoconjugates. As shown in Figure 1C, representative conjugates displayed a homogeneous distribution of drug content along the polymer population (as derived from the SEC elution profiles in UV–vis at 260 nm). These profiles conformed to the expected behavior according to size, as different conjugates exhibited slightly shorter retention times and broader peaks when compared with parental unconjugated/unmodified PGA (Figure 1C), in accordance with the enhanced M_w due to the incorporation of drugs.

2.2. Quantitative Characterization of Total Drug Loading and Free Drug Content in PGA–Drug Conjugates

Despite the lower reactivity of the aromatic amine present in AGM, we found the synthetic carbodiimide-activation methodology

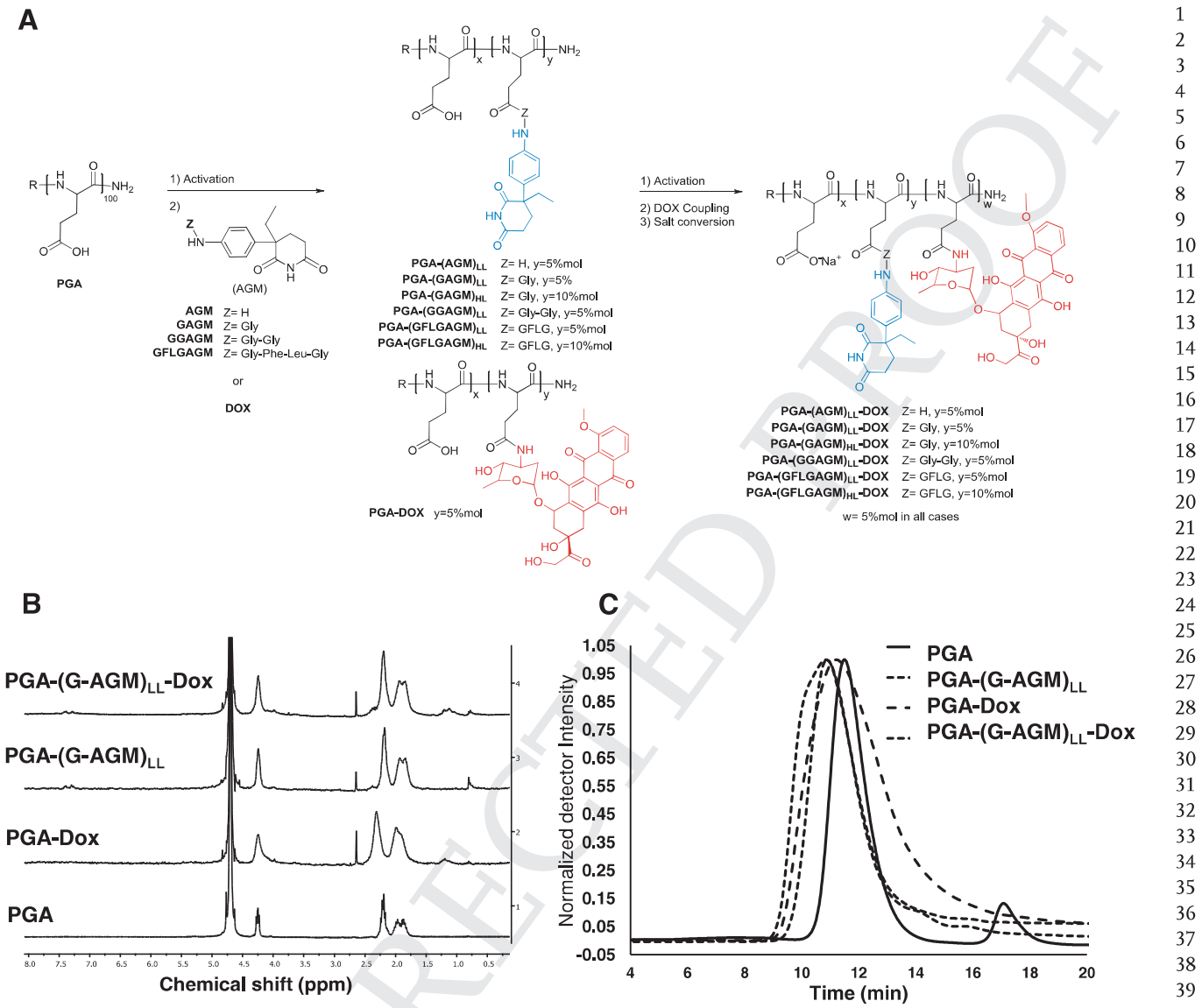

Figure 1. A) Synthetic route for the preparation of single and combination PGA-drug conjugates: 1) Carbodiimide-based carboxylic group activation. 2) Attachment of Dox or AGM (or derivatives) for single conjugates, and Dox coupling as the second drug in the combination conjugates. 3) Conversion into polycarboxilate form. B) Representative ^{1}H-NMR spectra (D_2O, 500 MHz) and C) representative SEC chromatograms for parental PGA (RI detection, peak at 17.1 corresponds to the counter-cation Na^+) and PGA-Dox, PGA-(G-AGM)$_{LL}$, and PGA-(G-AGM)$_{LL}$-Dox conjugates (UV at 260 nm).

to be a good and reproducible approach (Table 1) for both the single and combination conjugates. We noted that conjugation yield improved significantly when we first incorporated AGM with different peptidic linkers, and so we performed amide coupling through a primary peptidic amine rather than through the primary aromatic amine of the drug. We also noted efficient conjugation of Dox, except for combination conjugates bearing the GFLG-AGM moiety. Lower Dox loading in the presence of the bulky GFLG-AGM moiety may be due to steric hindrance, which can limit high levels of Dox incorporation. We also found that an SEC-based purification procedure ensured low levels of free-drug in the final conjugates ranging from 0.1% to 0.7% w/w for Dox and 0.2–1.1% w/w for AGM (Table 1). Absolute M_w analysis by analytical tandem SEC-MALS-RI proved difficult due to heterogeneity in drug loadings and the inherent nature of the conjugates, so we calculated the theoretical molecular weight of PGA conjugates according to the percentage of modification (range: 12.7–18.6 kDa).

2.3. Preliminary In Vitro Evaluation and Drug Release Kinetics of PGA Conjugates

To assess the biological implications of different drug linkers and drug ratios in the synthesized conjugates, we undertook a wide-ranging preliminary in vitro screening of the PGA-AGM-Dox family of conjugates. This analysis also compared treatment with the various PGA-AGM conjugates and PGA-Dox as

Table 1. Characteristics of PGA-AGM-Dox polymer–drug conjugates.

Compound	Total drug[a] [%w/w]		Free drug[b] [%w/w to total drug]		M_w[c] [Da]	Total drug [%mol]	
	AGM	Dox	AGM	Dox	–	AGM	Dox
PGA	–	–	–	–	12 700	–	–
PGA-$(AGM)_{LL}$	6.8	–	1.1	–	13 600	4.0	–
PGA-$(G\text{-}AGM)_{LL}$	9.1	–	0.9	–	13 900	4.7	–
PGA-$(G\text{-}AGM)_{HL}$	17.8	–	0.7	–	15 450	9.5	–
PGA-$(GG\text{-}AGM)_{LL}$	10.8	–	0.9	–	14 200	4.4	–
PGA-$(GFLG\text{-}AGM)_{LL}$	10.4	–	0.2	–	14 800	2.5	–
PGA-$(GFLG\text{-}AGM)_{HL}$	18.8	–	0.4	–	15 650	4.8	–
PGA-(Dox)	–	14.2	–	0.1	14 800	–	3.9
PGA-$(AGM)_{LL}$-Dox	8.1	15.8	0.8	0.4	16 700	5.8	4.8
PGA-$(G\text{-}AGM)_{LL}$-Dox	7.8	20.1	1.1	0.3	17 600	5.61	6.5
PGA-$(G\text{-}AGM)_{HL}$-Dox	20.1	12.7	1.0	0.4	18 900	13.1	4.4
PGA-$(GG\text{-}AGM)_{LL}$-Dox	7.6	18.9	0.9	0.2	17 300	3.8	6.0
PGA-$(GFLG\text{-}AGM)_{LL}$-Dox	12.4	7.1	0.3	0.7	15 800	3.2	2.0
PGA-$(GFLG\text{-}AGM)_{HL}$-Dox	24.2	7.6	0.4	0.7	18 600	7.4	2.6

[a]Determined by UV–vis (AGM) and HPLC (Dox); [b]Determined by HPLC; [C]Determined by aqueous SEC MALLS-RI for the sodium salt form of PGA. Mw of the polymer–drug conjugates were estimated from total drug loading.

two separate species added simultaneously (i.e., drugs were not present in the same polymeric chain).

Cell viability assays in the MCF-7ca breast cancer cell line demonstrated higher cytotoxicity for the combination conjugates PGA-$(GG\text{-}AGM)_{LL}$-Dox (**Figure 2**B), PGA-$(G\text{-}AGM)_{LL}$-Dox (Figure 2C), and PGA-$(G\text{-}AGM)_{HL}$-Dox (Figure 2D) when compared with the single PGA-Dox and PGA-AGM parent conjugates alone or in a physical combination (**Table 2**). The PGA-$(AGM)_{LL}$-Dox (Figure 2A), PGA-$(GFLG\text{-}AGM)_{LL}$-Dox (Figure 2E), and PGA-$(GFLG\text{-}AGM)_{HL}$-Dox (Figure 2F) did not display high toxicity compared to PGA-Dox at tested concentrations. We found evidence of poor Dox release in the combination conjugates bearing GFLG-AGM (see Figure S13, Supporting Information), which is a requisite for cell toxicity. This fact may be due to intramolecular hydrophobic interactions that could trigger steric hindrance and, therefore, restricted access of proteases to the Dox linker. Of note, the physical combination of single drug conjugates administered at the same time (Figure 2A,E,F) did mediate an enhanced cytotoxic effect when compared to the combination conjugates. However, whole body pharmacokinetics and conjugate interaction with biological barriers in vivo play a determinant role and, therefore, the administration of two single conjugates to a patient will not ensure that both drugs will arrive at the same target cell at the desired ratio and within the required period, making this treatment strategy ultimately inefficient for our selected molecular targets.

As previous studies demonstrated significant synergism between AGM and Dox in the different breast cancer cells when incorporated within the same nonbiodegradable polymeric carrier,[12–14] we computed the combination index (CI) for our new biodegradable systems against MCF-7-ca.[29] These calculations discovered no synergistic effects when we treated cells with both drugs as separate single conjugates (Figure S1, Supporting Information—PGA-$(AGM)_{LL}$ + PGA-Dox, PGA-$(GG\text{-}AGM)_{LL}$ + PGA-Dox, PGA-$(G\text{-}AGM)_{LL}$ + PGA-Dox, and PGA-$(G\text{-}AGM)_{HL}$ + PGA-Dox), except for the PGA-$(GFLG\text{-}AGM)_{LL}$ and PGA-Dox treatment, which provided the lowest CI value of 0.3. However, we did observe high levels of synergism (CI < 1) for the PGA-$(G\text{-}AGM)_{LL}$-Dox (0.32), PGA-$(G\text{-}AGM)_{HL}$-Dox (0.32), and PGA-$(GG\text{-}AGM)_{LL}$-Dox (0.33) combination conjugates (Figure S1, Supporting Information), with a weaker synergistic effect observed for PGA-$(GFLG\text{-}AGM)_{LL}$-Dox (0.56).

We noted that the presence of the linker drastically modified the in vitro cytotoxic effects; the addition of small, short, and flexible Gly or Gly–Gly linkers led to enhanced results when compared to direct linkage of AGM or through the more bulky GFLG linker. Additionally, we assessed cell toxicity of two highly synergistic conjugates found in the previous study in murine 4T1 breast cancer cells as a first step toward studying conjugate antitumor activity in an orthotopic immunocompetent mammary tumor mouse model. The PGA-$(G\text{-}AGM)_{LL}$-Dox (IC_{50} = 0.0034 mg mL^{-1} Dox equiv.) and PGA-$(G\text{-}AGM)_{HL}$-Dox (IC_{50} = 0.0033 mg mL^{-1} Dox equiv.) conjugates presented higher cytotoxicity compared to the single conjugate PGA-Dox (IC_{50} = 0.0084 mg mL^{-1} Dox equiv.) (**Figure 3**A,B, respectively, and Figure S2, Supporting Information). We also assessed cell toxicity of PGA-$(AGM)_{LL}$-Dox as a control for nonsynergistic effect (Figure 3C) and, as expected, this combination conjugate displayed a higher IC_{50} value (0.012 mg mL^{-1} Dox equiv.) than the combination conjugates bearing the Gly spacer. In general, we observed a more pronounced cytotoxic activity in 4T1 cells than in MCF-7-ca, probably due to the higher level of Cathepsin B activity in 4T1 cells,[14] which degrades the peptidic polymer–drug linkers and the poly-L-glutamic acid carrier. Subsequent CI value calculations found strong synergism for the PGA-$(G\text{-}AGM)_{HL}$-Dox conjugate (CI = 0.176) (Figure S2, Supporting Information).

We also evaluated drug release kinetics in presence of Cathepsin B for the PGA-$(G\text{-}AGM)_{LL}$-Dox, PGA-$(G\text{-}AGM)_{HL}$-Dox, and PGA-$(AGM)_{LL}$-Dox conjugates (Figure 3D–F), finding three different release profile scenarios as a consequence of drug loadings and linker type. The PGA-$(G\text{-}AGM)_{LL}$-Dox conjugate displayed a significantly faster and higher release of AGM (13% after 72 h) in contrast to Dox (7%) during the same time period. However, the PGA-$(G\text{-}AGM)_{HL}$-Dox conjugate released higher amount of Dox (12% at 72 h) as compared to lower levels of AGM (3%) over the same time. Meanwhile, the PGA-$(AGM)_{LL}$-Dox conjugate displayed a simultaneous release profile for both drugs (≈10%) over 72 h. PGA-$(G\text{-}AGM)_{HL}$-Dox and PGA-$(G\text{-}AGM)_{LL}$-Dox differ only in their level of AGM loading, with higher loading significantly diminishing drug release kinetics, perhaps due to structural modifications in the polymer chain. However, we noted a similar cytotoxic effect

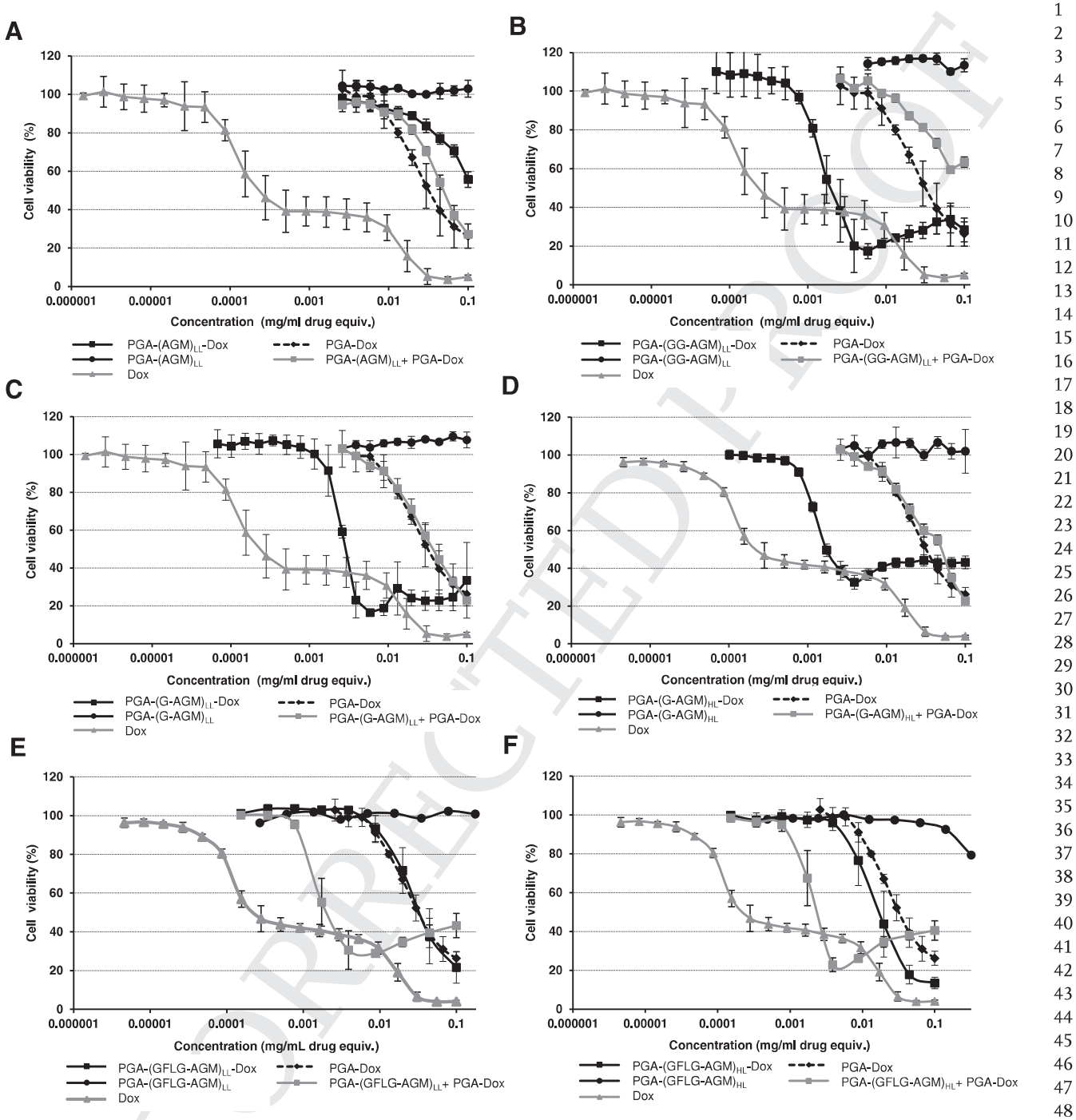

Figure 2. Cell toxicity study of polymer drug conjugates in MCF-7-ca cells. Cell viability measured by MTS assay after 72 h of treatment. A) PGA-$(AGM)_{LL}$-Dox, B) PGA-$(GG\text{-}AGM)_{LL}$-Dox, C) PGA-$(G\text{-}AGM)_{LL}$-Dox, D) PGA-$(G\text{-}AGM)_{HL}$-Dox, E) PGA-$(GFLG\text{-}AGM)_{LL}$-Dox, and F) PGA-$(GFLG\text{-}AGM)_{HL}$-Dox. Every assay is displayed with its corresponding single conjugates and Dox as free drug control. Data expressed as mean ± SEM, at least $n = 3$ experiments per treatment.

for both LL and HL conjugates, possibly mediated through different molecular mechanisms. While high Dox release from the PGA-$(G\text{-}AGM)_{HL}$-Dox can enhance cytotoxicity, high AGM release from the PGA-$(G\text{-}AGM)_{LL}$-Dox conjugate may enhance cell sensitivity to Dox[13,14] and provide a synergistic effect even given the lower levels of Dox release. Aromatase inhibitors such as AGM promote apoptosis[22] and this may also sensitize cancer cells to Dox treatment. In a direct comparison between PGA-$(AGM)_{LL}$-Dox and PGA-$(G\text{-}AGM)_{LL}$-Dox conjugates, which only differ in the addition of the small flexible Gly linker, enhanced AGM release seems to be related with structural alteration promoted by Gly. In terms of drug

Table 2. Summary of main physicochemical and biological descriptors of the selected polymer–drug conjugates.

Polymer–drug conjugate	Cytotoxicity human MCF-7-ca	Cytotoxicity murine 4T1	Size (R_H) (By number)	Cellular uptake	Secondary structure trend	Antitumor activity	Drug release	SANS
PGA-$(AGM)_{LL}$-Dox	Low (IC_{50} = 0.53 mg mL^{-1})	Sparingly (IC_{50} = 0.012 mg mL^{-1})	≈100 nm	High	Alpha-helix	Noneffective	Simultaneous	Larger, noncompact aggregates. No evidence of internal ordering
PGA-(G-AGM)$_{LL}$-Dox	High (IC_{50} = 0.003 mg mL^{-1})	High (IC_{50} = 0.0034 mg mL^{-1})	≈20 nm	Low	Random coil	Effective	AGM first and faster	Larger compact aggregates. Some internal ordering
PGA-(G-AGM)$_{HL}$-Dox	High (IC_{50} = 0.0017 mg mL^{-1})	High (IC_{50} = 0.0033 mg mL^{-1})	≈4 nm	Low	Alpha-helix	Highly effective	Dox first and faster	Smaller, more compact aggregates. No evidence of internal ordering
PGA-(GG-AGM)$_{HL}$-Dox	High (IC_{50} = 0.0011 mg mL^{-1})	N/A	≈7 nm	Low	Random coil	N/A	N/A	Large compact aggregates. Internally ordered

synergism, we found that Gly presence induced synergism while the absence of Gly brings drug antagonism.

Drug release required the strategic design of the family of polypeptide–drug conjugates toward lysosomotropic delivery, where the enzymatic degradation of the polymeric chain will release the active agents at the desired site of action. This not only improves therapeutic efficiency but also reduces unwanted off-target side effects. The degradation process requires efficient cellular uptake and adequate access of the endopeptidase to the linker,[30] with accessibility directly related with the 3D spatial disposition of the polypeptide. This in turn is influenced by structural factors such as conjugated moieties,[31] drug loadings,[32] drug ratios,[33] linking chemistry, and physicochemical descriptors mediating the nanobiointerface.[10,34] At this point, in vitro behavior of the conjugates cannot be explained by taking into account drug loadings and linking chemistry solely, although it seems clear that under the same PGA-Dox linking chemistry and drug loading, incorporation of AGM at different ratios or through different linkers could explain the observed results.

2.4. Antitumor Evaluation and Biodistribution of Selected Conjugates in a 4T1 Orthotopic Breast Cancer Murine Model

The conjugation of active agents to a biodegradable polymer provides distinct advantages over conventional monotherapy

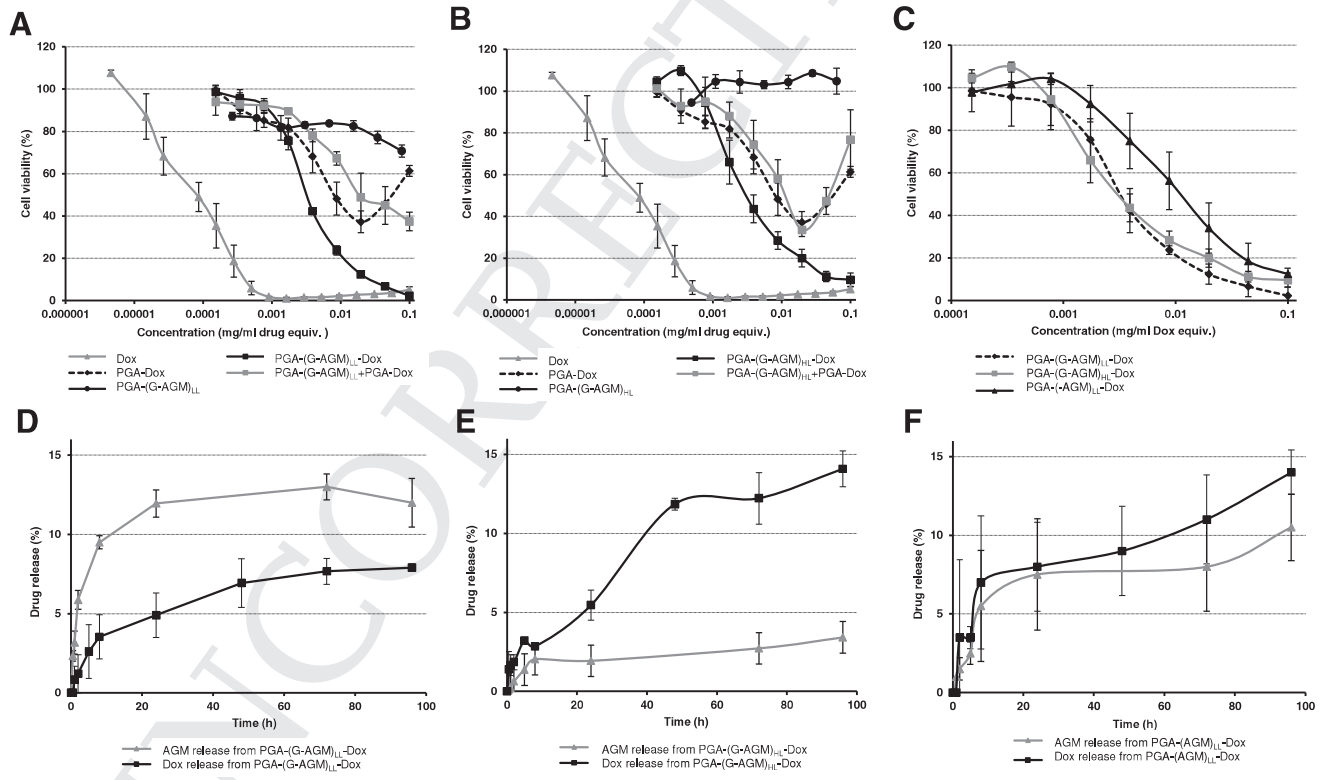

Figure 3. Cell toxicity analysis of the polymer drug conjugates A) PGA-$(G\text{-}AGM)_{LL}$-Dox and B) PGA-$(G\text{-}AGM)_{HL}$-Dox in 4T1 cells. C) Comparative study of cell toxicity of PGA-$(G\text{-}AGM)_{LL}$-Dox, PGA-$(G\text{-}AGM)_{HL}$-Dox, and PGA-$(AGM)_{LL}$-Dox. Cell viability measured by MTS assay after 72 h of the treatment. Drug release kinetics in presence of Cathepsin B of D) PGA-$(G\text{-}AGM)_{LL}$-Dox, E) PGA-$(G\text{-}AGM)_{HL}$-Dox, and F) PGA-$(AGM)_{LL}$-Dox. Data expressed as mean ± SEM, at least $n = 3$ experiments per treatment.

strategies. These include passive accumulation of the combination conjugate in solid tumors thanks to the EPR effect[5] as well as the simultaneous delivery of both drugs at the tumor site of action.[9] Given tumor complexity, modulating the activity of two pathways will often provide greater therapeutic effects than monotherapies. In addition, polymer conjugation permits enhanced blood circulation times that allows sustained bioavailability and conjugate accumulation in tumor vessels, so leading to enhanced therapeutic output. The orthotopic mouse 4T1 breast tumor model has several characteristics that make an attractive experimental model to mimic breast cancer[35] including the well vascularized nature of the tumor,[36] which is a prerequisite for the EPR effect.

In order to explore the antitumor effect of the nanosystems under study, we randomly split mice inoculated with 4T1 cells into representative groups and scheduled three treatments every three days with selected combination conjugates and their corresponding single conjugates at 10 mg kg^{-1} Dox equiv. We administered Dox as a free agent in a control group at the maximum nonlethal dose (3 mg kg^{-1}).[14] Analysis of tumor growth along time (**Figure 4**A) demonstrated high intragroup uniformity allowing us to effectively evaluate the antitumor effect of different treatments. Treatment with the single conjugates bearing AGM, Dox, the addition of either single conjugate, or free Dox did not significantly affect tumor growth. However, we observed a synergistic antitumor effect in animals treated with the PGA-(G-AGM)$_{LL}$-Dox and PGA-(G-AGM)$_{HL}$-Dox combination conjugates, as compared with the single conjugates (alone or added simultaneously) and controls (unconjugated PGA or PBS) (Figure 4A).

We assessed safety profiles for all tested polymer–drug conjugates via the study of body weight, general wellbeing, behavior, and histopathology of specific organs. We did not observe significant alterations in body weight of treated animals (Figure 4C) and histological study of the kidney and liver displayed no pathological tissue alterations related with any conjugate-based treatment, confirming the in vivo safety of this family of polymer–drug conjugates (see Figure S14, Supporting Information, for details). Subsequent analysis of survival rates (Figure 4B) demonstrated that PGA-(G-AGM)$_{LL}$-Dox and PGA-(G-AGM)$_{HL}$-Dox treated mice survived longer than other treated mice (controls or single treatments).

We next studied biodistribution and pharmacokinetics for a representative conjugate with high antitumor activity (PGA-(G-AGM)$_{HL}$-Dox) and compared the treatment with conventional Dox intravenous (i.v.) administration as a monotherapy in the 4T1 tumor model. Passive tumor accumulation reached a maximum accumulation time at 4 h after i.v. administration (59-fold in comparison with free Dox, Figure 4D). We also detected conjugate accumulation in the heart and spleen, although at a significantly lower level (Figure 4E). Given the small size of the conjugate tested, we also expected kidney and liver accumulation due to renal excretion as well as clearance by the reticuloendothelial system (Figure 4E), which may be promoted by the altered conformation of the combination conjugate.[37] To perform the pharmacokinetics study, we analyzed plasma samples of treated animals at different times (basal, 0.5, 1, 4, and 24 h) and quantified Dox accumulation by HPLC (Figure 4F). We observed a similar blood circulation time profile for the combination polymer conjugate in comparison with free Dox. However, while we did not detect Dox at 30 min postadministration of the free Dox form, we did detect Dox following combination conjugate treatment, resulting in a nine-times higher PGA-(G-AGM)$_{HL}$-Dox accumulation half-life ($t½\alpha$ = 0.4 h) when compared to free Dox ($t½\alpha$ = 0.09 h) (Figure 4G). These data agree with previous studies.[14,37]

2.5. Physicochemical Evaluation of Selected Conjugates and Cellular Uptake

The conjugation of single drugs and combinations of drugs influences conjugate size and conformation, and these effects modify the biophysical properties and thus the pharmacokinetic and biodistribution profile of the resultant conjugate. Conjugated moieties introduce new spatial and charged elements that change the electrostatic equilibrium of the whole anionic polypeptide.[10] While the behavior of our conjugates in the animal model can be explained by the drug release kinetics, drug synergism profiles, and the in vitro analyses, any correlation between drug loadings, linking chemistry, and in vivo fate remains unsolved. Such correlations are driven by an intricate and complex interplay of interconnected factors. The lack of descriptive elements to predict biological output within this family of polymer–drug conjugates motivated us to carry out a more detailed physicochemical characterization of the conjugates, looking at conformational and structural/morphological features that might allow us to rationalize the observed biological performance.

At the molecular level, secondary structure analysis by CD (**Figure 5**A) demonstrated that PGA-(G-AGM)$_{LL}$-Dox clearly deviated from the expected random coil conformation of the polyanionic PGA toward a partial alpha-helix conformation.[38] We performed measurements in 10×10^{-3} M phosphate buffer (pH = 7.4) in order to avoid the influence of pH on PGA secondary structure. Therefore, we attributed the observed changes in conformation exclusively to the modifications performed.[39] PGA-(AGM)$_{LL}$-Dox demonstrated a trend toward an alpha-helix conformation. The native secondary structure expected for PGA backbone seems to govern the overall conformation with increasing hydrophilic Gly linker length. Interestingly, the percentage of modification also influenced the disruptive effect of the linker; comparisons between PGA-(G-AGM)$_{LL}$-Dox and PGA-(G-AGM)$_{HL}$-Dox demonstrated that the significant trend to partial alpha-helix structure can only be attributable to the increase of G-AGM moiety loading. G-AGM appears to partially shift the secondary structure to alpha-helix again, even more markedly than in the parent conjugate with direct attachment of drugs.

In order to ascertain how these observations at molecular level correlate with the polymer–drug conjugate conformations adopted in solution, we studied selected samples by SANS. The scattering data obtained for PGA-(AGM)$_{LL}$-Dox, PGA-(G-AGM)$_{LL}$-Dox, PGA-(G-AGM)$_{HL}$-Dox, and PGA-(GG-AGM)$_{LL}$-Dox are shown on a log–log plot in Figure 5E. We fitted the data according to a broad peak model[40] (see Figure S15, Supporting Information, for fitting details and complete analysis). The predominant conformation of PGA in its protonated state

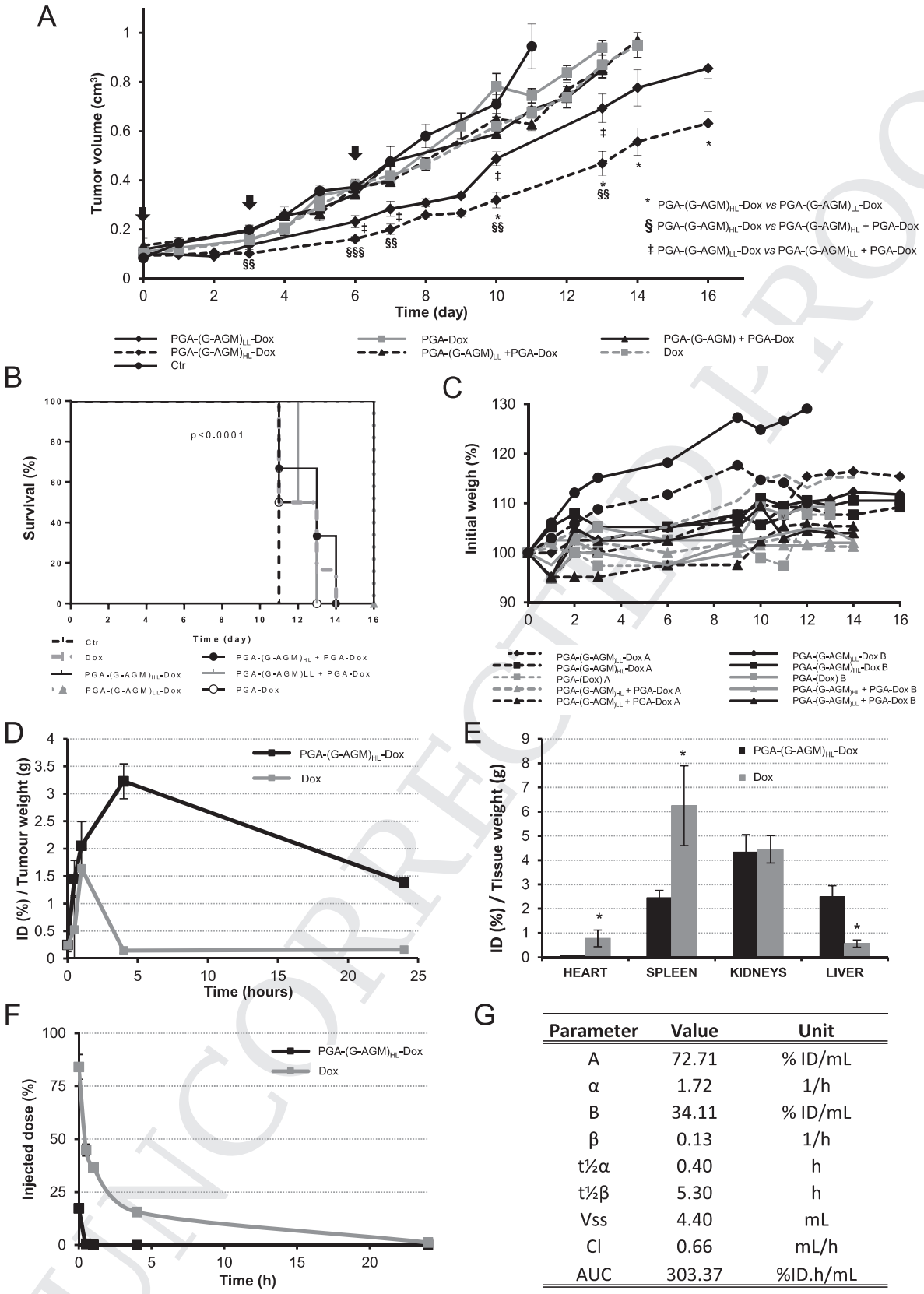

G

Parameter	Value	Unit
A	72.71	% ID/mL
α	1.72	1/h
B	34.11	% ID/mL
β	0.13	1/h
t½α	0.40	h
t½β	5.30	h
Vss	4.40	mL
Cl	0.66	mL/h
AUC	303.37	%ID.h/mL

Figure 4. Antitumor activity and safety of PGA-(G-AGM)$_{LL}$-Dox and PGA-(G-AGM)$_{HL}$-Dox in an orthotopic 4T1 breast tumor mice model. A) The combination conjugates PGA-(G-AGM)$_{HL}$-Dox inhibited tumor volume growth more than PGA-(G-AGM)$_{LL}$-Dox, the simple conjugate or the combination

in solution at low concentration is a helical structure at the molecular scale, giving rise to rod-like molecules at acidic pH, while random coil is the preferred conformation in the carboxylate form (pH > pK_a).[39] These helixes associate in solution to form larger clusters that have an internal structure arising from alignment of the individual rod-like PGA molecules. Apart from the conjugate PGA-(G-AGM)$_{HL}$-Dox (68 nm), the total size of the clusters is outside of the accessible Q range for SANS, in agreement with the volume and/or intensity data obtained by DLS where the large-sized aggregates population has a much pronounced contribution to the overall size distribution (Figure S16, Supporting Information). However, detailed information can be provided on the alignment and spacing of molecules within the clusters. Due to the low drug loading and the single contrast (H-conjugate in D_2O), the PGA polymer backbone dominated the observed scattering. Hence, the SANS data provide information on how the drug and linker conjugation affect the PGA solution structure. The higher slope of the low Q scattering data (n) for the PGA-(GG-AGM)$_{LL}$-Dox, PGA-(G-AGM)$_{LL}$-Dox, and PGA-(G-AGM)$_{HL}$-Dox conjugates compared to PGA-(AGM)$_{LL}$-Dox suggests a fundamental difference in structure of the aggregates formed by these conjugates. Fitting parameters for PGA-(GG-AGM)$_{LL}$-Dox, PGA-(G-AGM)$_{LL}$-Dox, and PGA-(G-AGM)$_{HL}$-Dox are indicative of more collapsed clusters (i.e., in the globular state with less free space within the scattering body, see Figure S15, Supporting Information, for full discussion). For the PGA-(AGM)$_{LL}$-Dox conjugate, fitting data suggested a more open Gaussian-like structure at this length scale (i.e., that the clusters are likely to be less densely internally packed). This would be in agreement with the measured size distributions by number shown in Figure 5B, where the large aggregates are outweighed, and hence the predominant clusters sizing follow the trend PGA-(GG-AGM)$_{LL}$-Dox < PGA-(G-AGM)$_{HL}$-Dox < PGA-(G-AGM)$_{LL}$-Dox < PGA-(AGM)$_{LL}$-Dox with the latter showing R_h size distributions of 100 nm in both number or intensity plots, in agreement with cryo-transmission electron microscopy (TEM) (Figure 5C). The Gly linker introduces a hydrophilic character in the AGM construct, and computed Log$P$ values (a measure of hydrophobicity or hydrophilicity) for AGM (1.46), G-AGM (0.09), and GG-AGM (−1.06) demonstrated a significant reduction of hydrophobicity of AGM upon Gly incorporation. Hence, PGA-(AGM)$_{LL}$-Dox had the highest hydrophobic character, displayed the highest propensity to aggregate (Figure S17, Supporting Information), and also had the largest cluster size.

In the high Q region of the SANS data, the experiment probes the arrangement of chains within the cluster. Conjugates with low loading of AGM attached by a Gly–Gly and Gly linker both gave a small, broad peak (centered at Q_0 = 0.062 and 0.043 Å^{-1}, respectively) in the scattering data (Inset in Figure 5E). This peak corresponds to a length scale of around 100–140 Å ($2\pi/Q_0$) within the structure, which is attributed to regular spacing of adjacent rigid molecules within the cluster. The absence of a peak for PGA-(AGM)$_{LL}$-Dox and PGA-(G-AGM)$_{HL}$-Dox indicated a loss of short range order within the aggregate, presumably as the effect of chain–chain charge interactions is outweighed by the excluded volume requirements, and drug solvent effect of the attached drugs. The smaller Q_0 value for PGA-(G-AGM)$_{LL}$-Dox agrees with the lower flexibility of the linking group (compared to PGA-(GG-AGM)$_{LL}$-Dox) causing a greater perturbation of the PGA conformation. The peak observed in PGA-(G-AGM)$_{LL}$-Dox is lost when increasing the AGM loading to form PGA-(G-AGM)$_{HL}$-Dox. This further highlights drug-caused perturbation of PGA clusters.

Taken together, these data indicate that direct conjugation of the AGM molecules (in addition to the Dox present in all conjugates) disrupts the ability of the PGA to adopt its preferred solution conformation.[27] The flexibility introduced by the Gly–Gly linker allows the character of the polymer backbone to dominate the structures formed, with the conjugate containing Gly–Gly linker (most flexible) showing the scattering most similar to that of pure PGA (peak is present).[27] With the Gly linker, at low G-AGM loading the Gly affords sufficient flexibility for the PGA to retain its internal ordering (peak) and the overall aggregated morphology (n^{-3}). These data are consistent with CD spectroscopy that reports a range of helical content of the conjugates as discussed above (Figure 5A). Comparing the SANS data for these two conjugates, we start to see the influence of the additional G-AGM on the secondary structure. At low G-AGM loading the overall structure remains broadly similar to that expected for pure PGA, as described above. At high loading PGA-(G-AGM)$_{HL}$-Dox, packing of the individual molecules in the clusters is less ordered, (loss of peak). This is presumably due to a reduction in PGA–PGA charge repulsions, which keep the molecules separated by the characteristic distance indicated by the peak at high Q. This lessened repulsion allows for closer association of the conjugate molecules, and the clusters become smaller and more globular (turnover at low Q). This smaller globular structure is a favorable result, as it is apparent that conjugates with such morphologies, as shown by SANS, give lowest IC$_{50}$ values (Figures S1 and S2, Supporting Information).

For the PGA-(AGM)$_{LL}$-Dox, PGA-(G-AGM)$_{LL}$-Dox, and PGA-(G-AGM)$_{HL}$-Dox, the CD, DLS, and SANS data can help to correlate structure, conformation, and drug release studies with the biological output (Table 2). Results from in vitro and in vivo experiments suggest that the drug release profile is the main factor in the antitumor activity of this family of conjugates. However, for PGA-(AGM)$_{LL}$-Dox exists evidence of a higher helical conformation and propensity to aggregate with the biggest cluster sizes (Figure 5B and Figure S17, Supporting Information) and degradation of the PGA-(±G)-drug links is not

Q13 of the simple conjugates (PGA-(G-AGM)$_{HL}$ + PGA-Dox). Data represent mean ± SEM. Statistical significance was determined using an ANOVA t-test, (***p < 0.005, **p < 0.01). B) Kaplan–Meier survival curves by treatment demonstrating improved overall survival for PGA-(G-AGM)$_{HL}$-Dox and PGA-(G-AGM)$_{LL}$-Dox. The long-rank test demonstrated significant differences (p < 0.0001). C) Animal body weight did not significantly decrease along the experiment. Biodistribution study of PGA-(G-AGM)$_{HL}$-Dox and Dox was studied in an orthotopic 4T1 breast tumor mice following i.v. injection D) in a tumor and E) in blood until 24 h, and in heart, spleen, kidney, and liver at 24 h. F) The conjugate remained longer than Dox in the bloodstream allowing sustained state for better tumor accumulation. G) Pharmacokinetic parameters obtained from blood sample of mice i.v. administered with PGA-(G-AGM)$_{HL}$-Dox analyzed by a bicompartment model (n = 5).

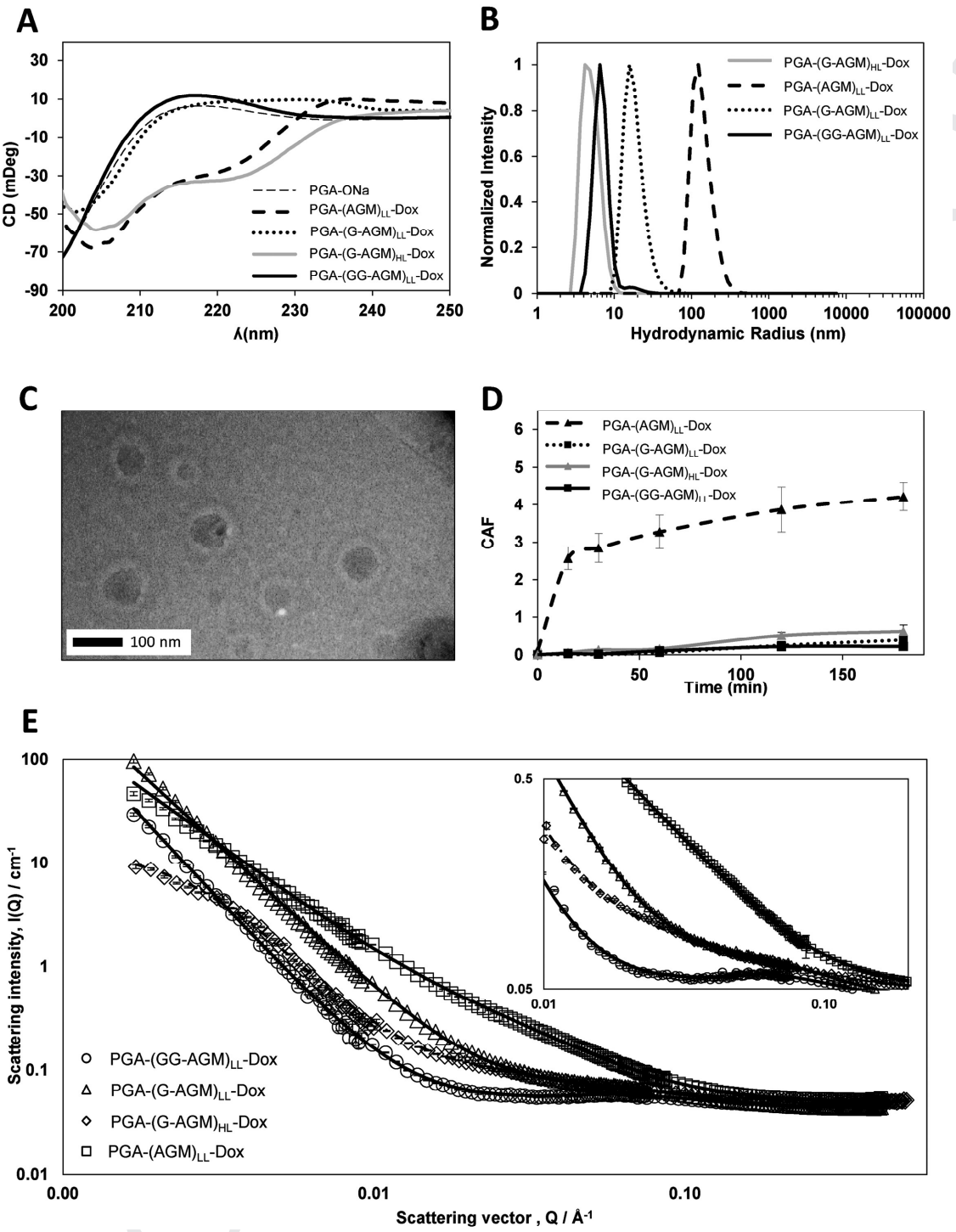

Figure 5. Physicochemical characterization of selected combination conjugates PGA-$(AGM)_{LL}$-Dox, PGA-$(G\text{-}AGM)_{LL}$-Dox, and PGA-$(G\text{-}AGM)_{HL}$-Dox. A) Circular dichroism data on selected conjugates in phosphate buffer 10×10^{-3} M, pH = 7.4 at 0.6 mg mL^{-1}. B) Size distribution graphs in number obtained by DLS in PBS at 2 mg mL^{-1}. C) Representative Cryo-TEM image of PGA-$(AGM)_{LL}$-Dox in H_2O at 2 mg mL^{-1}, scale bar is 100 nm. D) Cellular uptake study of the selected conjugates by flow cytometry. Results are represented as the average of cell associated fluorescence (CAF) ± SEM. ($n = 3$). E) SANS profiles and fitting.

(or certainly is less) inhibited. However, although this conjugate also displays by far the most efficient cellular uptake along the family, the simultaneous drug release and subsequent drug antagonism translates into low cytotoxicity. Combined with the identical polymer–drug linkages this accounts for the similar release profiles for both drugs. For the PGA-$(G\text{-}AGM)_{LL}$-Dox, AGM was released preferentially to Dox. The more strongly helical structure of the individual PGA-$(G\text{-}AGM)_{LL}$-Dox conjugate

molecules indicated by CD supports the lower accessibility of Dox and ordered spacing structures within the clusters suggests structure with greater accessibility for the cathepsin B cleaving group. It is more difficult to reconcile the release data for the PGA-(G-AGM)$_{HL}$-Dox conjugate: lower release of AGM and high release of Dox. CD reports a helical structure at the molecular level, SANS reports disordered clusters of molecules that are smaller and more densely packed than PGA-(G-AGM)$_{LL}$-Dox. Neither technique probes the detailed packing of the AGM around the PGA helix, but SANS assessments indicate that, at high G-AGM content, intermolecular interactions are AGM, rather than PGA, dominated. Intramolecular or indeed intermolecular AGM–AGM interactions may somehow be screening the linkers. This might also be indicative of nonrandom distribution of the drug along the PGA chain at the higher loading either at outset, or induced as the drug loading changes at very low release levels. More detailed structural studies at key timepoints would be required to resolve these possibilities.

3. Conclusions

We have designed a wide family of single and combination polymer–drug conjugates aiming for efficient antitumor treatment for breast cancer. Within the present family of PGA–AGM–Dox conjugates, we ratify the importance of the presence of both drugs in the same polymeric carrier that secures their codelivery to the same cell. Of note, we paid special attention to the interplay between biological behavior and determinant physicochemical properties. As expected drug ratio is a key feature ruling conjugate activity as seen for PGA-(G-AGM)$_{HL}$-Dox vs PGA-(G-AGM)$_{LL}$-Dox in this case. More importantly, we discovered that the presence of the small and flexible Gly linker (the smallest amino acid, involving less than 1% of the total molecular weight of the conjugate) plays a decisive role in the structure of the whole macromolecule and hence significantly influences biological activity. The introduction of Gly induces a significant shift in drug release kinetics, size, secondary structure, and internal arrangement of the polypeptidic backbone as derived from the intensive CD, DLS, and SANS studies. The different configuration for Gly linker introduction (G or GG) between the polymer and AGM seems to modify the spatial disposition of the conjugate in such a way as to modify the disposition of the conjugate for the protease cleavage allowing a differential release of AGM vs Dox and consequently determining the final therapeutic output. It is clear that the kinetics of drug release is one of the major physicochemical descriptors to take into account when designing combination therapeutics.

As seen within this work, the choice of linkers employed in the conjugation of active agents in a combination-polymer-drug conjugate can endow the complex macromolecular system with enhanced properties. In our family of conjugates the best performance was seen with PGA-(G-AGM)$_{HL}$-Dox, conjugate bearing a 2:1 (AGM: Dox) molar ratio and Gly as AGM linker. This combination conjugate showed significantly greater antitumor effects than PGA-(G-AGM)$_{LL}$-Dox (1:1 AGM: Dox molar ratio) and even more remark performance if compared with those with a direct AGM conjugation.

Our results lay the groundwork to move toward the efficient design of newer conjugates with more adequate linkers allowing enhanced spatiotemporal control on release profiles, seeking for synergistic effects and, therefore, improved antitumor effects. Our results also highlight the importance of an exhaustive supramolecular characterization to adequately compare in vitro and in vivo assessments.

4. Experimental Section

Cell Culture Conditions (MCF-7-ca and 4T1): Human estrogen-dependent breast cancer cell line MCF-7-ca (human aromatase-transfected) was ceded from the Tenovus Centre for Cancer Research at Cardiff University and the 4T1 breast cancer cell line 4T1 was obtained from ATTC (EU). MCF-7-ca cells were maintained in DMEM supplemented with 10% heat inactivated steroid-deprived fetal bovine serum (SFBS) (Thermo-Fisher Scientific, USA), 10^{-9} M of oestradiol (Sigma-Aldrich, Spain, UE) and 0.75 mg mL^{-1} of geneticin G418 (Thermo-Fisher Scientific, USA) over standard cell culture conditions (37 °C and 5% CO_2). SFBS was prepared as was previously described. 4T1 cells were maintained in RPMI supplemented with 10% heat inactivated fetal bovine serum over standard tissue culture conditions.

Cell Viability Assays: Cell lines were seeded in sterile 96-wells microtiter plates at the concentration of 12 500 cells cm^{-2} for MCF-7-Ca and 6250 cells cm^{-2} for 4T1. Plates were incubated for 24 h and then free drugs and the conjugates were tested at the final concentrations ranging from 0 to 0.1 mg mL^{-1} of drug equivalents. After 72 h of treatment cell viability was measured using the Cell Titer 96 Aqueous nonradioactive cell proliferation assay (Promega, Corporation, Spain, UE) in accordance with the manufacturer's instructions. The optical density of each well was measured at 490 nm using a Wallac 1420 Workstation (PerkinElmer, MA, USA). Cell viability was expressed as a percentage of the viability of untreated control cells.

Cellular Uptake Studies: Uptake assay was performed in MFC7-Ca cell line at two different temperatures, 37 and 4 °C. Cells were seeded in sterile six-wells plates at concentration of 32 000 cells cm^{-2} and incubated for 24 h. A cathepsin B inhibitor, Leupeptin (PanReac AppliChem, VWR, UE), was added to each well at 100×10^{-6} M 30 min before the incubation of the polymer conjugates (PGA-(AGM)$_{LL}$-Dox, PGA-(G-AGM)$_{LL}$-Dox, PGA-(GG-AGM)$_{LL}$-Dox, and PGA-(G-AGM)$_{HL}$-Dox in order to avoid polymer degradation. To perform the 4 °C uptake experiment, cells were preincubated at 4 °C during 30 min before addition of the treatments. 12 µg mL^{-1} of each polymer were tested at different time points (0–180 min). After that, medium was removed and two washes with PBS 0.1 wt% BSA (bovine serum albumin, Sigma-Aldrich, Spain, UE) were performed and finally cells were scraped and collected in 500 µL of PBS 0.1 wt% BSA. In order to detect the fluorescence into the cells, a FC500 MCL Flow Cytometer (Beckman-Coulter, CA, USA) was used. The cell associated fluorescence (CAF) was calculated based on the following formula (CAF = percentage positive cells x fluorescence level). The real uptake by endocytosis is the difference between the uptake at 37 and at 4 °C.

Orthotopic 4T1 Murine Breast Cancer Model: All the animal experiments were carried out in accordance with the guidelines established by the European communities council directive (86/609/ECC) and by Spanish Royal Decree 1201/2005 and were approved by the institutional Animal Care and Use Committee. Food and water were provided ad libitum during whole experiments in all cases and general aspect, behavior, and body weight were evaluated daily to ensure animal wellness. Six to eight weeks female Balb/c mice used for all the experimental procedures were purchased from Harlan Laboratories Inc. (Spain, EU). Tumor induction was performed by injecting 5×10^5 4T1 cells suspended in 100 µL of Matrigel in the second left mammary fat pad under inhalatory anesthesia (2.5% sevoflurane in 100% oxygen).

Antitumor Activity of Polymer Drug Conjugates: After 8 d of cell inoculation, when tumor size reached 0.1 cm^3, mice were split in representative groups and the conjugates were injected i.v. in three single doses of 10 mg Kg^{-1} Dox equivalents every three days. Free Dox was dissolved in saline and used as a control of free drug, administered at 3 mg kg^{-1} following the same schedule. Tumors were measured every 3 d with a digital caliper and volumes were obtained considering spheroid growth, applying the formula (height/2 x length/2 x width/2)^3 x (4/3 Pi). Once tumors reached 1.0 cm^3 (16 d after first treatment), mice were sacrificed under CO_2 atmosphere and blood, main organs as well as tumors were collected for later histopathological analysis. Kaplan–Meier survival curves were performed using GraphPad.

Biodistribution of PGA-(G-AGM)$_{HL}$-Dox Combination Conjugate: Mice bearing 0.1 cm^3 of tumor (developed as previously detailed) were used for biodistribution study. Single dose of 10 mg Kg^{-1} of Dox equivalents of the conjugate was i.v. administered and groups of animals (n = 6) were sacrificed at different time points (0, 8, 24, 48, and 72 h). Blood was collected and main organs and tumor were carefully and systematically excised, frozen, and storage at –80 °C until further analysis.

Organs and tumor were suspended in 2 mL of cold PBS and vigorously mixed by the use of an Ultraturrax mixer. pH of resultant homogeneous mix was adjusted to 8.5 by adding some drops of 1 M ammonium formate buffer and then extracted three times with 5.0 mL of a mixture of CH_3Cl/iPrOH 4:1 v/v. Aqueous phases were discarded and supernatants were concentrated till dryness under N_2 stream. Final residues were dissolved in 100 µL of HPLC-grade MeOH and samples were analyzed by RP-HPLC following the same method for Free Drug determination already described. Final fluorescent measurements related to Dox were standardized according tissue weight.

Half-Life of Conjugate in Plasma: Blood from biodistribution experiment was centrifuged (4000 rpm, 10 min, r.t.) and plasma was collected. 100 µL of plasma was made up to 1.0 mL with milliQ water and pH was fixed to 8.5 as previously explained. Liquid–liquid extraction was carried out three times with 5.0 mL of a mixture of CH_3Cl/iPrOH 4:1 v/v. Organic phases were dried under N_2 stream and suspended as already explained and analyzed by RP-HPLC under the same experimental conditions than for Free Drug determination.

Pharmacokinetics Analysis: The pharmacokinetics analysis was performed by nonlinear regression using the SOLVER function of Microsoft Excel[41] software as described before.[42] The pharmacokinetic parameters analyzed were A, B, ALPHA, BETA, Cl (D/AUC), Vss apparent terminal half-life, and AUC.

Supporting Information

Supporting Information is available from the Wiley Online Library or from the author.

Acknowledgements

J.J.A.-C. and C.D. contributed equally to this work. This work was supported by the European Research Council (grant ERC-CoG-2014-648831 "MyNano"), the Spanish Ministry of Science and Innovation (CTQ2010-18195, SAF2013-44848-R, BES-2008-006801, IPT-2012-0712-010000, Programa I3), GENTxGENT and Generalitat Valenciana (ACOMP2013/186). Part of the equipment employed in this work has been funded by Generalitat Valenciana and cofinanced with FEDER funds (PO FEDER of Comunitat Valenciana 2014–2020). ILL is acknowledged for support through provision of beam time and support for travel. Authors also want to thank Prof Ruth Duncan for helpful discussion, Dr. Stuart P. Atkinson for his collaboration in paper preparation and English revision, Dr. Amaya Niño for helping in the SANS samples measurements, Dr. Ralf Schweins for the SANS technician support, and Dr. Miguel Ángel Morcillo for his help in the PK study analysis. This work benefited also from the use of the SasView application, originally developed under NSF award DMR-0520547. SasView contains code developed with funding from the European Union's Horizon 2020 research and innovation program under the SINE2020 project, Grant Agreement No, 654000.

Conflict of Interest

The authors declare no conflict of interest.

Keywords

breast cancer, combination therapy, polymer therapeutics, polymer–drug conjugates, polypeptides

Received: February 5, 2018
Revised: March 15, 2018
Published online:

[1] a) W. Dai, X. Wang, G. Song, T. Liu, B. He, H. Zhang, X. Wang, Q. Zhang, *Adv. Drug Delivery Rev.* **2017**, *115*, 23; b) B. He, C. Lu, G. Zheng, X. He, M. Wang, G. Chen, G. Zhang, A. Lu, *J. Cell Mol. Med.* **2016**, *20*, 2231.
[2] D. R. Vogus, V. Krishnan, S. Mitragotri, *Curr. Opin. Colloid Interface Sci.* **2017**, *31*, 75.
[3] R. A. Burrell, N. McGranahan, J. Bartek, C. Swanton, *Nature* **2013**, *501*, 338.
[4] A. Ronson, A. Tvito, J. M. Rowe, *Expert Opin. Orphan Drugs* **2017**, *5*, 369.
[5] a) H. Maeda, *Bioconjugate Chem.* **2010**, *21*, 797; b) H. Maeda, K. Tsukigawa, J. Fang, *Microcirculation* **2016**, *23*, 173; c) T. Ojha, V. Pathak, Y. Shi, W. E. Hennink, C. T. W. Moonen, G. Storm, F. Kiessling, T. Lammers, *Adv. Drug Delivery Rev.* **2017**, *119*, 44.
[6] a) A. Nino-Pariente, V. J. Nebot, M. J. Vicent, *Curr. Pharm. Des.* **2016**, *22*, 1274; b) M. Tajes, E. Ramos-Fernandez, X. Weng-Jiang, M. Bosch-Morato, B. Guivernau, A. Eraso-Pichot, B. Salvador, X. Fernandez-Busquets, J. Roquer, F. J. Munoz, *Mol. Membr. Biol.* **2014**, *31*, 152.
[7] a) F. Canal, J. Sanchis, M. J. Vicent, *Curr. Opin. Biotechnol.* **2011**, *22*, 894; b) R. Duncan, *Curr. Opin. Biotechnol.* **2011**, *22*, 492.
[8] R. Duncan, M. J. Vicent, *Adv. Drug Delivery Rev.* **2013**, *65*, 60.
[9] F. Greco, M. J. Vicent, *Adv. Drug Delivery Rev.* **2009**, *61*, 1203.
[10] O. Zagorodko, J. J. Arroyo-Crespo, V. J. Nebot, M. J. Vicent, *Macromol. Biosci.* **2017**, *17*, 22.
[11] A. E. Nel, L. Madler, D. Velegol, T. Xia, E. M. V. Hoek, P. Somasundaran, F. Klaessig, V. Castranova, M. Thompson, *Nat. Mater.* **2009**, *8*, 543.
[12] M. J. Vicent, G. Francesca, N. R. I. , P. Alison, G. P. C. , D. Ruth, *Angew. Chem., Int. Ed. Engl.* **2005**, *44*, 4061.
[13] F. Greco, M. J. Vicent, S. Gee, A. T. Jones, J. Gee, R. I. Nicholson, R. Duncan, *J. Controlled Release* **2007**, *117*, 28.
[14] . C. Deladriere, *PhD Thesis*, University of Valencia, Spain **2013**.
[15] R. Duncan, *J. Drug Targeting* **2017**, *25*, 759.
[16] S. Hehir, N. R. Cameron, *Polym. Int.* **2014**, *63*, 943.
[17] B. Weinstock-Guttman, K. V. Nair, J. L. Glajch, T. C. Ganguly, D. Kantor, *J. Neurol. Sci.* **2017**, *376*, 255.
[18] R. Duncan, *J. Controlled Release* **2014**, *190*, 371.
[19] a) E. Bernabeu, M. Cagel, E. Lagomarsino, M. Moretton, D. A. Chiappetta, *Int. J. Pharm.* **2017**, *526*, 474; b) J. Zhao, E. J. Koay,

T. Li, X. Wen, C. Li, *Wiley Interdiscip. Rev.: Nanomed. Nanobiotechnol.* **2017**, https://doi.org/10.1002/wnan.1497.

[20] H. Baabur-Cohen, L. I. Vossen, H. R. Kruger, A. Eldar-Boock, E. Yeini, N. Landa-Rouben, G. Tiram, S. Wedepohl, E. Markovsky, J. Leor, M. Calderon, R. Satchi-Fainaro, *J. Controlled Release* **2017**, *257*, 118.

[21] a) E. Markovsky, B.-C. Hemda, S.-F. Ronit, *J. Controlled Release* **2014**, *187*, 145; b) A. Eldar-Boock, K. Miller, J. Sanchis, R. Lupu, M. J. Vicent, R. Satchi-Fainaro, *Biomaterials* **2011**, *32*, 3862.

[22] S. R. Khan, A. Baghdasarian, P. H. Nagar, R. Fahlman, P. Jurasz, K. Michail, N. Aljuhani, A. G. Siraki, *Chem.-Biol. Interact.* **2015**, *239*, 129.

[23] S. R. D. Johnston, M. Dowsett, *Nat. Rev. Cancer* **2003**, *3*, 821.

[24] F. Zhang, M.-R. Liu, H.-T. Wan, *Biol. Pharm. Bull.* **2014**, *37*, 335.

[25] M. J. Vicent, E. Perez-Paya, *J. Med. Chem.* **2006**, *49*, 3763.

[26] V. P. R. Chichili, V. Kumar, J. Sivaraman, *Protein Sci.* **2013**, *22*, 153.

[27] a) J. D. Nickels, S. Perticaroli, G. Ehlers, M. Feygenson, A. P. Sokolov, *J. Biomed. Mater. Res. A* **2015**, *103*, 2909; b) M. Rinaudo, A. Domard, *J. Polym. Sci., Polym. Lett. Ed.* **1977**, *15*, 411.

[28] R. Duncan, in *Polymeric Drug Delivery Systems* (Ed: G. S. Kwong), Marcel Dekker, New York **2005**, p. 1.

[29] T. C. Chou, *Pharmacol. Rev.* **2006**, *58*, 621.

[30] V. Turk, V. Stoka, O. Vasiljeva, M. Renko, T. Sun, B. Turk, D. Turk, *Biochim. Biophys. Acta, Proteins Proteomics* **2012**, *1824*, 68.

[31] a) V. Gimenez, C. James, A. Arminan, R. Schweins, A. Paul, M. J. Vicent, *J. Controlled Release* **2012**, *159*, 290; b) G. Mezo, J. Remenyi, J. Kajtar, K. Barna, D. Gaal, F. Hudecz, *J. Controlled Release* **2000**, *63*, 81.

[32] M. Q. Li, W. T. Song, Z. H. Tang, S. X. Lv, L. Lin, H. Sun, Q. S. Li, Y. Yang, H. Hong, X. S. Chen, *ACS Appl. Mater. Interfaces* **2013**, *5*, 1781.

[33] a) Y. J. Pu, S. Chang, H. Yuan, G. Wang, B. He, Z. W. Gu, *Biomaterials* **2013**, *34*, 3658; b) Y. Bae, T. A. Diezi, A. Zhao, G. S. Kwon, *J. Controlled Release* **2007**, *122*, 324.

[34] S. Van, S. K. Das, X. H. Wang, Z. L. Feng, Y. Jin, Z. Hou, F. Chen, A. Pham, N. Jiang, S. B. Howell, L. Yu, *Int. J. Nanomed.* **2010**, *5*, 825.

[35] B. A. Pulaski, S. Ostrand-Rosenberg, *Current Protocol in Immunology* **2001**, Ch. 20, Unit 20.2.

[36] K. C. Mei, J. Bai, S. Lorrio, J. T. W. Wang, K. T. Al-Jamal, *Biomaterials* **2016**, *106*, 276.

[37] A. Duro-Castano, R. M. England, D. Razola, E. Romero, M. Oteo-Vives, M. A. Morcillo, M. J. Vicent, *Mol. Pharm.* **2015**, *12*, 3639.

[38] J. J. Lai, Y. B. Huang, *RSC Adv.* **2015**, *5*, 48856.

[39] A. Duro-Castano, V. J. Nebot, A. Niño-Pariente, A. Armiñán, J. J. Arroyo-Crespo, A. Paul, N. Feiner-Gracia, L. Albertazzi, M. J. Vicent, *Adv. Mater.* **2017**, *29*, 1702888.

[40] F. Horkay, B. Hammouda, *Colloid Polym. Sci.* **2008**, *286*, 611.

[41] Y. Zou, H. Fu, S. Ghosh, D. Farquhar, J. Klostergaard, *Clin. Cancer Res.* **2004**, *10*, 7382.

[42] A. Aguilar, M. C. Montejo, M. Caamaño, F. R. Martín, *Biofarmacia y Farmacocinética*, 2nd ed., Elsevier, **2014**.

